RSC Advances

PAPER

View Article Online
View Journal | View Issue

Cite this: *RSC Adv.*, 2023, **13**, 14268

Synthesis and characterization of ammonium-based protic ionic liquids for carbon dioxide absorption†

Asyraf Hanim Ab Rahim,[ab] Normawati M. Yunus, *[ab] Zahirah Jaffar,[ab] Muhammad Faizadmesa Allim,[b] Nurhidayah Zulakha Othman Zailani,[ab] Shazri Amirah Mohd Fariddudin,[b] Noraini Abd Ghani[ab] and Mursyidah Umar[c]

A series of ammonium-based protic ionic liquids (APILs) namely ethanolammonium pentanoate [ETOHA][C5], ethanolammonium heptanoate [ETOHA][C7], triethanolammonium pentanoate [TRIETOHA][C5], triethanolammonium heptanoate [TRIETOHA][C7], tributylammonium pentanoate [TBA][C5] and tributylammonium heptanoate [TBA][C7] was synthesized *via* proton transfer. Their structural confirmation and physiochemical properties namely thermal stability, phase transition, density, heat capacity (C_p) and refractive index (RI) have been determined. Specifically, [TRIETOHA] APILs have crystallization peaks ranging from −31.67 to −1.00 °C, owing to their large density values. A comparison study revealed the low C_p values of APILs in comparison to monoethanolamine (MEA) which could be advantageous for APILs to be used in CO_2 separation during recyclability processes. Additionally, the performance of APILs toward CO_2 absorption was investigated by using a pressure drop technique under a pressure range of 1–20 bar at 298.15 K. It was observed that [TBA][C7] recorded the highest CO_2 absorption capacity with the value of 0.74 mole fraction at 20 bar. Additionally, the regeneration of [TBA][C7] for CO_2 absorption was studied. Analysis of the measured CO_2 absorption data showed marginal reduction in the mole fraction of CO_2 absorbed between fresh and recycled [TBA][C7] thus proving the promising potential of APILs as good liquid absorbents for CO_2 removal.

Received 28th February 2023
Accepted 3rd May 2023

DOI: 10.1039/d3ra01345f

rsc.li/rsc-advances

Introduction

The utilization of natural gas as an alternative fuel is essential in order to mitigate global climate change caused by significant carbon dioxide (CO_2) emission resulting from fossil fuel combustion. According to Safari and co-workers, natural gas plays a vital role as a transition fuel in our process of dealing with high energy demand.[1] Generally, natural gas contains a mixture of various gases such as methane (CH_4), nitrogen (N) and CO_2.[2] The presence of CO_2 in natural gas normally leads to pipeline corrosion due to formation of carbamic acid and reduces the burning velocity due to its high specific capacity. Therefore, highly efficient technology for CO_2 removal from natural gas is essential to improve the heating value of the natural gas streamline.

One of the common techniques for CO_2 removal is *via* chemical absorption system where the reversible chemical reactions occurred conveniently at low temperatures and high pressure.[3] Since decades ago, aqueous alkanolamine solutions such as monoethanolamine (MEA) and diethanolamine (DEA) were extensively used due to their low cost, safe to handle and accessibility.[3,4] However, the utilization of alkanolamine solutions is limited to their highly volatile and corrosive properties, in addition to their high energy consumption for absorbent regeneration process.[5] Dawson and co-workers also reported the loss of small amount of DEA due to its volatile property which likely leads to the pipeline corrosion issue.[6]

The interest in utilizing ionic liquids (ILs) as solvents for CO_2 absorption has been growing mainly due to their unique properties which are flexible designability,[7] high thermal stability, wide liquidous range, negligible vapor pressure and non-flammability.[8] The extremely low vapor pressure of ILs suggests that losing of liquid absorbent during recyclability process could be avoided. Since the last decades, hundreds of literature related to the room temperature ILs (RTILs) for CO_2 solubility were published, mainly involving class of imidazolium,[9] pyridinium[10] and pyrrolidinium.[11] These cations combine with anions namely bis(trifluoromethylsulfonyl)imide (NTf_2) and hexafluorophosphate (PF_6) provide high CO_2 uptake

[a]*Institute of Contaminant Management, Centre for Research in Ionic Liquid (CORIL), Universiti Teknologi PETRONAS, 32610, Seri Iskandar, Perak, Malaysia. E-mail: normaw@utp.edu.my*

[b]*Department of Fundamental and Applied Sciences, Universiti Teknologi PETRONAS, 32610, Seri Iskandar, Perak, Malaysia*

[c]*Department of Petroleum Engineering, Faculty of Engineering, Universitas Islam Riau, Jalan Kaharuddin Nasution, No. 113 Pekanbaru, Riau, 28284, Indonesia*

† Electronic supplementary information (ESI) available. See DOI: https://doi.org/10.1039/d3ra01345f

compared to nitrate (NO_3) and dicyanamide (DCN).[12] However, despite incredible performance of RTILs, these types of ILs suffer some drawbacks. The synthesis and purification steps are lengthy with some ILs requiring complicated synthesis route thus increasing the production cost.[13]

Amino acid based ILs (AAILs) were first introduced by Fukumoto and co-workers in an effort to gain functionalized ILs through simple methods.[14] On the other hand, the presence of amines in AAILs is expected to be able to improve the CO_2 absorption capacity as its mechanism mimics the MEA and DEA but with better recovery yield due to its low vapor pressure. Apart from that, AAILs are biodegradable, less corrosive, stable against oxidative degradation and offer fast kinetic CO_2 absorption due to their low viscosity values. Numerous AAILs such as 1-(3-aminopropyl)-3-(2-aminoethyl)imidazolium alaninate [Apaeim][Ala],[15] trihexyl(tetradecyl)ammonium lysinate [N_{66614}][Lys],[16] 1-ethyl-3-methylimidazolium alanate [EMIM][Ala] and 1-ethyl-3-methylimidazolium glycinate [EMIM][Gly][17] have been utilized for CO_2 absorption. Nevertheless, some AAILs are highly viscous thus reducing the rate of CO_2 absorption capacity.

Nowadays, protic ILs (PILs) had gained attention due to their simple synthesis route and affordable reactants.[18] According to Greaves and Drummond, PILs are formed through proton transfer that occur between Brønsted acid and Brønsted base.[19] Apart from a straightforward synthesis process, PILs also do not undergo decomposition stage before boiling point due to the simple mechanism of proton transfer from cation to anion.[19] This results in the reformation the original acid and base neutral species. Our previous work had reported the potential ammonium-based protic ILs for CO_2 absorption in which bis(2-ethylhexyl) ammonium butyrate [BEHA][BA] had demonstrated higher mole fraction of CO_2 absorption capacity, 0.486 in comparison to less than 0.30 by [C_4py][NTf_2] at the same reaction conditions.[10,20]

In light of this, this paper reports the continuation of our work of synthesis, characterization and CO_2 absorption with six new ammonium-based PILs (APILs) containing carboxylate anions as shown in Fig. 1. All APILs had undergone characterizations including structural confirmation while thermal properties analyses comprising thermal stability, phase transition, heat capacity, refractive index and density were also completed and reported. The measurements of CO_2 absorption for each APIL at pressures 1 to 20 bars and temperature 298.15 K were conducted. The recyclability and reusability of the APIL that displayed the highest CO_2 absorption capacity were also conducted and discussed herein.

Experimental

Materials

All chemicals of analytical grade were used without additional purification process for APILs synthesis and CO_2 absorption. The CAS number, source and chemical purity are as follow: ethanolamine (141-43-5, Merck, 98%), triethanolamine (102-71-6, Merck, 98%), tributylamine (102-82-9, Merck, 98.5%), pentanoic acid (109-52-4, Merck, 99%) and heptanoic acid (111-14-8, Merck, 99%).

Synthesis of APILs

The synthesis of APILs was conducted based on our previous method as shown in Fig. 2 with slight modifications.[20] In this work, the reaction was set up in an ice bath. An equal molar of acid was added dropwise into 50 mL round bottom flask containing 0.5 mol of base. The mixture was then continuously stirring at 250 rpm in room temperature for 24 hours to ensure

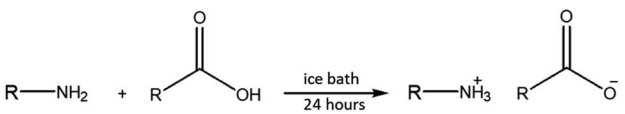

Fig. 2 General synthesis pathway for APILs.

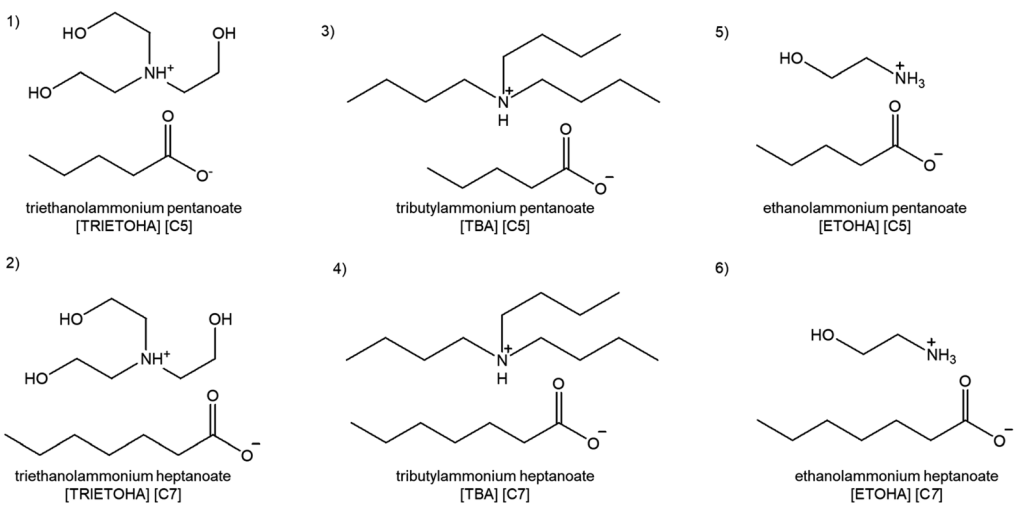

Fig. 1 Chemical structure of synthesized APILs.

all reactants were completely reacted. The resulting viscous liquid was dried using rotary evaporator and store in vacuum cabinet until further use.

The combination of acids and bases produced six APILs namely ethanolammonium pentanoate [ETOHA][C5], triethanolammonium pentanoate [TRIETOHA][C5], tributylammonium pentanoate [TBA][C5], ethanolammonium heptanoate [ETOHA][C7], triethanolammonium heptanoate [TRIETOHA][C7] and tributylammonium heptanoate [TBA][C7], which all exist as liquid at room temperature.

Characterization

Structural confirmation. The structural characterization for APILs was conducted by analysing ^{1}H spectrum gained from Nuclear Magnetic Resonance (NMR) by Bruker Advance III 500Mhz. The analysis was carried out at room temperature subjected to different deuterated solvent. About 5.0 mg of APIL was dissolved in 650 μL of deuterated solvent. The chemical shifts were reported in part per million (ppm) with TMS as an internal standard. Multiplicities are abbreviated as follow: s = singlet, d = duplet, t = triplet and m = multiplet. Meanwhile, all ^{1}H NMR spectra of APILs are available in the ESI data.†

Water content. The water content analysis of APILs was performed by adding 1.0 mL of sample into reagent of Volumetric Karl Fischer and Stromboli Oven, model V30 from Mettler Toledo.

[ETOHA][C5]: ^{1}H NMR (500 MHz, $CdCl_3$): δ 3.762 [t, 2H, CH_2-OH], 2.993 [t, 2H, CH_2-NH_2], 1.516 [t, 2H, CH_2-COOH], 1.470 [m, 2H, CH_2], 1.323 [m, 2H, CH_2], 1.293, [t, 3H, CH_3], water content: 2.48%.

[ETOHA][C7]: ^{1}H NMR (500 MHz, $CdCl_3$): δ 3.753 [t, 2H, CH_2-OH], 2.972 [t, 2H, CH_2-NH_2], 2.098 [t, 2H, CH_2-COOH], 1.469 [m, 2H, CH_2], 1.295 [m, 6H, CH_2], 0.873, [t, 3H, CH_3], water content: 3.47%.

[TRIETOHA][C5]: ^{1}H NMR (500 MHz, $CdCl_3$): δ 3.739 [t, 6H, CH_2-OH], 2.983 [t, 6H, CH_2-NH_2], 2.173 [m, 2H, CH_2-COOH], 1.486 [m, 2H, CH_2], 1.326 [m, 2H, CH_2], 0.874, [t, 3H, CH_3], water content: 1.31%.

[TRIETOHA][C7]: ^{1}H NMR (500 MHz, $CdCl_3$): δ 3.726 [t, 6H, CH_2-OH], 2.957 [t, 6H, CH_2-NH_2], 2.161 [m, 2H, CH_2], 1.508 [t, 2H, CH_2-COOH], 1.270 [m, 6H, CH_2], 0.842 [t, 3H, CH_3], water content: 2.18%.

[TBA][C5]: ^{1}H NMR (500 MHz, $CdCl_3$): δ 2.633 [t, 6H, CH_2-NH_2], 2.078 [t, 2H, CH_2-COOH], 1.427 [m, 8H, CH_2], 1.214 [m, 8H, CH_2], 1.200 [t, 12H, CH_3], water content: 0.41%.

[TBA][C7]: ^{1}H NMR (500 MHz, $CdCl_3$): δ 2.644 [t, 6H, CH_2-NH_2], 2.071 [t, 2H, CH_2-COOH], 1.400 [m, 8H, CH_2], 1.187 [m, 12H, CH_2], 0.822 [t, 12H, CH_3], water content: 0.20%.

Thermal stability. Analysis on thermal stability of APILs was carried out by using thermogravimetric analyser (TGA), STA 6000 from PerkinElmer. Approximately, 5.0 mg of sample was place on a crucible pan and placed on sample holder. The sample was place under isothermal condition by heated up to 100 °C for 10 minutes to remove excess moisture. Then, the analysis was done at temperature range of 50–650 °C at the heating rate 10 °C min^{-1} under 20 mL min^{-1} nitrogen.

Density. The density (ρ) measurement of APILs was conducted by using 2mL-glass pycnometer. A known weight of glass pycnometer was filled with sample and the capillary glass stopper was inserted. The glass pycnometer containing sample was then immersed in water bath that was set up based on designated temperature for 15–20 minutes before weighted on weighing balance. The measurement was repeated three times under the same condition. The density of APILs was calculated based on eqn (1) as follows:

$$\rho_{\mathrm{APILs}} = \frac{(W_{\mathrm{APILs}} - W_{\mathrm{o}})}{V_{\mathrm{APILs}}} \quad (1)$$

where W_{APILs} is the weight of APILs with glass pycnometer W_{o} is the weight of empty pycnometer and V_{APILs} is the known volume of APILs (2.0 mL).

Refractive index. The refractive index of APILs was measured triplicate using ATAGO RX-5000 Alpha Digital Refractometer at temperature range of 293.15–333.15 K. A validation test was conducted using standard organic solvents provided by supplier to ensure the accuracy in sample measurement.

Viscosity. The viscosity of APILs was measured by using an Ubbelohde viscometer (2B, 1C and 3C) from Cannon Instrument Company. An Ubbelohde viscometer was placed in water bath set up to desired temperature. 12 mL of APILs was introduced into the reservoir then sucked through the capillary and measuring bulb. The kinematic viscosity (v) was determined by measuring the efflux time of the liquid to fall between two meniscus level in capillary and calculated based on eqn (2):

$$v = Kt \quad (2)$$

where K is the capillary viscometer characteristic constant and t is the efflux time in seconds. The kinematic viscosity data then was used to calculate the dynamic viscosity of APILs using eqn (3) as follows:

$$\eta = \rho \times v \quad (3)$$

In which η is dynamic viscosity, ρ is APILs density and v is kinematic viscosity value.

Phase transition. The phase transition analysis was conducted by using differential scanning calorimetry (DSC) from Mettler Toledo model DSC 1. Approximately 6.0 mg of sample was placed on aluminum pan and sealed. The testing was performed in temperature range −150 to 80 °C at 10 °C min^{-1} heating rate. The data for analysis was collected during second heating stage.

CO_2 absorption measurement

The solubility of CO_2 in APILs was conducted by utilizing pressure drop technique using a solubility cell. Fig. 3 shows the schematic diagram of solubility cell used in this study. Generally, the pre-weighted amount of APILs was loaded into 15 mL equilibrium cell and degassed using a vacuum pump. The equilibrium cell, made up from stainless steel was immersed in thermostatic water bath to maintain the temperature at 298.15 K. Meanwhile, the CO_2 in gas vessel was set up into desired

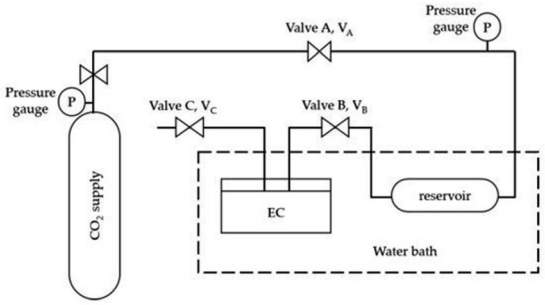

Fig. 3 Schematic diagram of solubility cell.

pressure in reservoir (V_A–V_B) and was allowed to stabilize. The CO_2 was then introduced into the equilibrium cell by opening V_B and the system was maintained at sufficient time (120–180 minutes) until it reached an equilibrium state.

The performance of APILs in CO_2 absorption was calculated based on eqn (4):

$$n_2 = \frac{P_{ini} V_{res}}{Z_i(P_{ini}, T_{ini}) R T_{ini}} - \frac{P_{eq}(V_{total} - V_{APILs})}{Z_{eq}(P_{eq}, T_{eq}) R T_{eq}} \quad (4)$$

where n_2 is number of moles of CO_2 absorbed by APILs, P_{ini} is initial pressure, V_{res} is the volume of CO_2 in reservoir (V_A–V_B), Z is the compressibility factor calculated by using Peng–Robison equation of state at selected pressure and temperature while R is the value of universal gas constant (0.0821 L atm K^{-1} mol^{-1}). In the meantime, P_{eq} and T_{eq} are representing equilibrium pressure and temperature, respectively. V_{total} indicates the total volume of CO_2 absorption system (V_A–V_C) while V_{APILs} is associated with volume of liquid absorbents. The volume of APILs was obtained by dividing the mass of APILs utilized before CO_2 adsorption with its density. In this work, the solubility of CO_2 in APILs was expressed in mole fraction x_{CO_2} and calculated based on eqn (5) as follows:

$$x_{CO_2} = \frac{n_{CO_2}}{n_{CO_2} + n_{APILs}} \quad (5)$$

in which n_{CO_2} is the number of moles CO_2 absorbed by APILS and n_{APILs} is the number of moles of APILs used the system.

Besides that, the solubility of CO_2 in APILs was determined by using Henry's law constant (K_H) in which the experimental data was fitted into linear regression of eqn (6):

$$P_{CO_2} = H x_{CO_2} \quad (6)$$

where x_{CO_2} is the physical absorption value, P_{CO_2} is the CO_2 partial pressure and H is K_H in APILs in bar.

Furthermore, ^{13}C NMR and FTIR spectroscopy analyses were conducted to evaluate the possible reaction pathway between CO_2 and APILs. In this study, both analyses were done after 20 minutes of CO_2 absorption process.

The recyclability of APILs towards CO_2 absorption was conducted according to the method suggested by Li and co-workers.[21] APILs was transferred into an evaporating flask in which CO_2 was released by using rotary evaporator at the temperature 333.15 K. The recycled APILs was left under vacuum for 2 hours prior to reuse in CO_2 absorption analysis. In this work, the recyclability test was conducted for a single cycle only.

Results and discussions

Thermal stability of APILs

TGA analysis was conducted in order to study the thermal decomposition behaviour of APILs. Basically, the APILs were categorized by the cation namely $[ETOHA]^+$, $[TRIETOHA]^+$ and $[TBA]^+$ to facilitate the findings discussion. Analysis on TG curves for all APILs showed similar pattern with sharp shouldering around 191.42–291.88 °C. In addition, the thermal stability of APILs increased with the alkyl chain of anion as shown in Table 1. This result is in agreement with work done by Chhotaray and co-workers in which they reported an improvement in thermal stability of lactam-based ILs as the number of anion carbon atom increased from formate to hexanoate.[22] Besides that, according to Othman Zailani *et al.*, the longer the anion alkyl chain, the higher the amount of energy required to

Table 1 The values of T_o and T_p for APILs

APILs	T_o (°C)	T_p (°C)
[ETOHA][C5]	162.2	191.42
[ETOHA][C7]	168.86	197.63
[TRIETOHA][C5]	256.18	280.71
[TRIETOHA][C7]	267.45	291.88
[TBA][C5]	137.4	168.31
[TBA][C7]	149.5	195.86

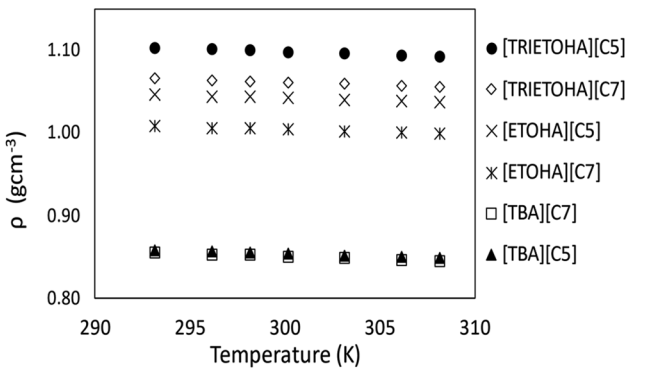

Fig. 4 Density of APILs at 293.15–333.15 K.

Table 2 Fitting parameters to correlate density of APILs and calculated SD

Ionic liquids	A_0	A_1	SD
[ETOHA][C5]	1.2164	−0.0006	0.0004
[ETOHA][C7]	1.7619	−0.0006	0.0006
[TRIETOHA][C5]	1.3105	−0.0007	0.0008
[TRIETOHA][C7]	1.2318	−0.0006	0.0008
[TBA][C5]	1.0447	−0.0006	0.0006
[TBA][C7]	1.0380	−0.0007	0.0004

Table 3 The values of molar mass, α, V, $S°$, U_{POT}, V_m, R_m and V_f for APILs

Temperature (K)	Molar mass (g mol^{-1})	$\alpha \times 10^{-4}$ (K^{-1})	$V_m \times 10^2$	$S°$ (J K^{-1} mol^{-1})	U_{POT} (K J mol^{-1})	V (nm^3)	R_m (cm^3 mol^{-1})	V_f (cm^3 mol^{-1})
[ETOHA][C5]	**163.21**							
293.15		5.9	1.572	355.0	470.9	0.261	43.33	113.9
296.15		5.9	1.575	355.5	470.7	0.261	43.33	114.1
298.15		5.9	1.578	356.0	470.5	0.262	43.37	114.4
300.15		5.9	1.580	356.5	470.3	0.262	43.39	114.6
303.15		5.9	1.582	357.0	470.1	0.263	43.39	114.9
306.15		5.9	1.585	357.6	469.9	0.263	43.40	115.1
308.15		5.9	1.588	358.2	469.7	0.264	43.42	115.4
313.15		5.9	1.591	358.9	469.4	0.264	43.40	115.7
323.15		6.0	1.602	361.0	468.6	0.266	43.44	116.7
333.15		6.0	1.610	362.8	468.0	0.267	43.43	117.6
[ETOHA][C7]	**191.27**							
293.15		3.7	1.901	422.9	448.4	0.316	51.73	138.3
296.15		3.7	1.905	423.8	448.1	0.316	51.76	138.7
298.15		3.7	1.908	424.5	447.9	0.317	51.79	139.0
300.15		3.7	1.912	425.3	447.7	0.318	51.84	139.4
303.15		3.7	1.915	426.0	447.5	0.318	51.84	139.7
306.15		3.7	1.918	426.5	447.3	0.319	51.82	140.0
308.15		3.7	1.921	427.0	447.2	0.319	51.83	140.2
313.15		3.7	1.925	427.9	446.9	0.320	51.79	140.7
323.15		3.7	1.937	430.4	446.2	0.322	51.81	141.9
333.15		3.7	1.947	432.5	445.6	0.323	51.77	142.9
[TRIETOHA][C5]	**251.32**							
293.15		6.9	2.301	505.9	427.1	0.382	64.67	165.5
296.15		6.9	2.307	506.9	426.9	0.383	64.72	165.9
298.15		6.9	2.312	508.0	426.6	0.384	64.79	166.4
300.15		6.9	2.316	508.9	426.4	0.385	64.84	166.8
303.15		6.9	2.319	509.6	426.3	0.385	64.81	167.1
306.15		6.9	2.323	510.4	426.1	0.386	64.80	167.5
308.15		6.9	2.329	511.7	425.8	0.387	64.89	168.1
313.15		7.0	2.337	513.2	425.4	0.388	64.90	168.8
323.15		7.0	2.354	516.7	424.7	0.391	64.95	170.4
333.15		7.0	2.366	519.1	424.1	0.393	64.86	171.7
[TRIETOHA][C7]	**279.37**							
293.15		5.7	2.650	577.9	412.3	0.440	74.22	190.7
296.15		5.7	2.655	578.8	412.1	0.441	74.24	191.1
298.15		5.8	2.658	579.7	411.9	0.441	74.29	191.6
300.15		5.8	2.661	580.4	411.8	0.442	74.28	191.9
303.15		5.8	2.664	581.0	411.7	0.442	74.22	192.2
306.15		5.8	2.668	581.8	411.5	0.443	74.20	192.63
308.15		5.8	2.673	582.8	411.4	0.444	74.24	193.1
313.15		5.8	2.681	584.5	411.0	0.445	74.23	194.0
323.15		5.8	2.691	586.4	410.7	0.447	74.00	195.1
333.15		5.9	2.715	591.5	409.8	0.451	74.15	197.4
[TBA][C5]	**287.48**							
293.15		7.3	3.340	720.8	389.3	0.555	87.52	246.5
296.15		7.3	3.350	722.9	389.1	0.556	87.56	247.4
298.15		7.3	3.357	724.3	388.9	0.557	87.60	248.1
300.15		7.3	3.361	725.1	388.8	0.558	87.55	248.5
303.15		7.4	3.365	725.9	388.6	0.559	87.42	249.0
306.15		7.4	3.370	727.1	388.5	0.560	87.34	249.7
308.15		7.4	3.375	728.2	388.3	0.560	87.32	250.2
313.15		7.4	3.387	730.5	388.0	0.562	87.25	251.4
323.15		7.5	3.415	736.4	387.2	0.567	87.21	254.3
333.15		7.5	3.445	742.6	386.4	0.572	87.17	257.3

Table 3 (*Contd.*)

Temperature (K)	Molar mass (g mol^{-1})	$\alpha \times 10^{-4}$ (K^{-1})	$V_m \times 10^2$	$S°$ (J K^{-1} mol^{-1})	U_{POT} (K J mol^{-1})	V (nm^3)	R_m (cm^3 mol^{-1})	V_f (cm^3 mol^{-1})
[TBA][C7]	**315.53**							
293.15		7.9	3.741	803.9	378.8	0.621	98.48	275.6
296.15		7.9	3.757	807.1	378.4	0.624	98.65	277.0
298.15		7.9	3.76.1	808.0	378.3	0.625	98.61	277.5
300.15		7.9	3.766	809.0	378.2	0.625	98.56	278.0
303.15		8.0	3.773	810.5	378.0	0.627	98.51	278.8
306.15		8.0	3.782	812.3	377.8	0.628	98.49	279.7
308.15		8.0	3.789	813.7	377.6	0.629	98.50	280.4
313.15		8.0	3.804	816.8	377.2	0.632	98.47	281.9
323.15		8.1	3.833	822.9	376.5	0.636	98.35	284.9
333.15		8.2	3.869	830.3	375.7	0.642	98.44	288.4

cleave the neighbouring bond.[23] Table 1 shows the thermal stability of APILs presented in the forms of onset (T_o) and decomposition temperatures (T_p). In particular, T_o is an intersection between baseline and tangent of sample weight against temperature while T_p indicates the temperature where the maximum weight loss occurred.[24] Further analysis revealed that APILs with [TRIETOHA]$^+$ cation possessed high values of T_o and T_p, signifying their superior thermal stability compared to [ETOHA]$^+$ and [TBA]$^+$ APILs and this finding could be attributed to the bulky size of [TRIETOHA]$^+$ in comparison to other cations.

Density of APILs

Generally, ILs density decreases gradually with increasing temperature.[25] Theoretically, elevated temperature weakens the intermolecular forces that exist between ions thus causing molecules to move apart from each other.[26] This phenomenon will increase the molecules volume which then will result in low density value of liquids at high temperatures. In this work, the APILs density measurement was conducted in triplicate and the result is shown in ESI data† (Table S1†). Fig. 4 shows the average density values of APILs at the temperature range of 293.15–333.15 K.

Previous study had shown that, the density of PILs for common cations is affected by the length of anion alkyl chain.[23] In this study, APILs with C7 anion own lower density values compared to APILs with C5 anion. Similar results were also reflected in the work conducted by Yunus and co-workers in which their density of PILs decreased with increasing of anion alkyl chain.[20] The reduction of density in longer alkyl chain of APIL was caused by an increasing in interionic separation and low packing efficiency in their elongated anion structure.[27] This contributed into an increasing of volume occupied by anion thus decreasing the density value of APILs with C7 anion. Besides that, less efficient packing structure of tributylammonium cation [TBA]$^+$ had resulted in low density values of by [TBA][C5] and [TBA][C7] in comparison to APILs with [ETOHA]$^+$ and [TRIETOHA]$^+$.

The value of APILs density was then fitted based on eqn (7) as follows:

$$\rho = A_0 + A_1 T \tag{7}$$

where ρ is the density (g cm^{-3}), T (K) is temperature while A_0 and A_1 are correlation coefficients calculated by using the method of least squares whereas standard deviation (SD) was calculated by using eqn (8):

$$\mathrm{SD} = \sqrt{\frac{\sum_{i}^{n_{DAT}} \left(Z_{expt} - Z_{calc}\right)^2}{n_{DAT}}} \tag{8}$$

in which Z_{expt} and Z_{calc} is experimental and calculated values, respectively and n_{DAT} is the number of experiment points. Table 2 shows the fitting parameters of eqn (7) to correlate APILs density and SD value.

In the meantime, the thermal expansion coefficient (α) was calculated by using eqn (9) and the data were tabulated in Table 3. Generally, α is defined as the expansion amount of substance in reaction to a change in temperature.[28] As oppose to previous work in which α increased as temperature increased,[29] based on Table 3, the changes of α in this study is insignificant. This indicates that the α of APILs is independent of temperature. At 298.15 K, the α of APILs are in the range of 3.7×10^{-4} to 7.9×10^{-4} K^{-1}, which is lower than common solvents such as acetone (1.10×10^{-3} K^{-1}), chloroform (1.27×10^{-3} K^{-1}) and ethyl acetate (1.38×10^{-3} K^{-1}).

$$\alpha_\rho = 1/\rho \times (\partial\rho/\partial T) = -(A_1)/(A_0 + A_1 T) \tag{9}$$

Besides that, the experimental density data of APILs allows the determination of molar volume (V_m) and molecular volume (V) according to eqn (10) and (11), respectively, while based on Glassier theory, the standard molar entropy ($S°$) and lattice energy (U_{POT}) can be estimated by using eqn (12) and (13).[30]

$$V_m = \frac{M}{\rho} \tag{10}$$

$$V = \frac{M}{\rho \times N} \tag{11}$$

$$S° = 1246.5 \times V + 29.5 \tag{12}$$

Table 4 Fitting parameters to correlate RI of APILs and calculated SD

Ionic liquids	A_2	A_3	SD
[ETOHA][C5]	1.5469	−0.0003	0.0002
[ETOHA][C7]	1.5455	−0.0003	0.0002
[TRIETOHA][C5]	1.5732	−0.0003	0.0005
[TRIETOHA][C7]	1.5744	−0.0003	0.0003
[TBA][C5]	1.5625	−0.0004	0.0001
[TBA][C7]	1.5631	−0.0004	0.0002

$$U_{POT} = 1981.2 \times (\rho/M)^{1/3} + 103.8 \quad (13)$$

Table 4 shows the values of V_m, V, S° and U_{POT} of APILs, calculated at 298.15–333.15 K. Based on Table 4, the values of V_m, V, and S° increase in the order of [ETOHA][C5] < [ETOHA][C7] < [TRIETOHA][C5] < [TRIETOHA][7] < [TBA][C5] < [TBA][C7] at all temperatures which are in accordance with the molar mass of the APILs. This indicates the apparent effect of molar mass towards V_m, V and S° instead of density value.[31] Further analysis showed [TBA][C7] owns the highest V_m possibly due to its large cation size. Meanwhile, the strong anion–cation interaction that existed in small cation like ETOHA had contributed into its low V_m value. The same trend was also reflected in their V and V_f values. In contrary, analysis on U_{POT} showed the opposite trend. For example, [TBA][C7] with the highest molar mass than other APILs has the lowest U_{POT} value. This could be due to its larger size than other APILs leading into less packing of its ions which results in low U_{POT}. This result is in line with the work done by Khan and co-workers in which their ILs with large paratoluene sulfonate anion had the lowest U_{POT} value.[30]

Other than that, for APILs with the same cation classification, the values of V_m, V and S° were observed to be strongly dependence on the chemical structure of the anion. It also has been identified that anion with longer alkyl chain (C7) has high V_m and V due to the presence of extra methylene group (–CH_2) in carboxylate anion. At 298.15 K, the difference of V value between C5 and C7 anion for $[ETOHA]^+$, $[TRIETOHA]^+$ and $[TBA]^+$ are 0.055, 0.057 and 0.068 nm^3, respectively. For comparison purpose, we calculated the difference in V for APILs from literature which are [BEHA][C5] and [BEHA][C7].[23] Correspondingly, the V difference between both APILs is 0.056 nm^3 which in agreement with data obtained in this study thus supporting the contribution of extra -CH_2 in C7 anion. Meanwhile, under different cation classification, the TBA-APILs own highest V_m, V and S° than TRIETOHA- and ETOHA-APILs due to the presence of CH_3 in $[TBA]^+$ cation.

Refractive index of APILs

The refractive index (RI) demonstrates the dielectric response to an electrical field induced by electromagnetic field. In this work, the RI APILs was studied at temperature range 293.15–333.15 K, and the results are plotted in Fig. 5. The RI value of APILs was listed in the ESI data (Table S2).† It is important to note that RI values are solely reported based on the measured water contents

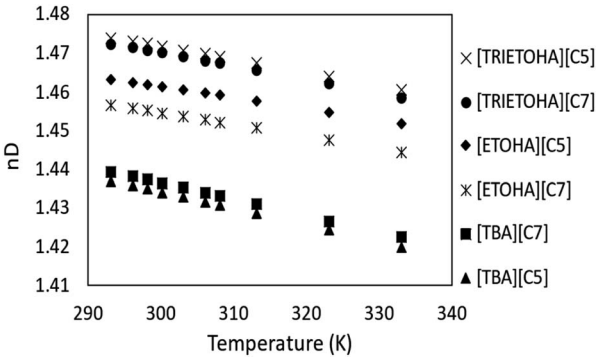

Fig. 5 The RI plot for APILs at temperature range 293.15–333.15 K.

of APILs. Based on Fig. 5, the values of RI for each APIL show a decreasing trend as temperature increases. These results are in line with the findings reported by Marcinkowski *et al.*[32]

The trend of RI is also in agreement with temperature dependence of APILs density with the exception of APIL with [TBA] cation. As for RI values, the trend is in the order of [TRIETOHA][C5] > [TRIETOHA][C7] > [ETOHA][C5] > [ETOHA][7] > [TBA][C7] > [TBA][C5]. According to Seki and co-workers, the RI was not affected by cation molecular weight[33] as the value decreased with increasing in number of carbon in anion which can be seen in TRIETOHA and ETOHA-based APILs. However, the order of RI is not retained for TBA-based APILs as it decreased with decreasing in anion molecular weight.

The RI of synthesized APILs was also fitted by least squares method using the linear eqn (14) while SD was calculated based on eqn (7). In eqn (14), A_2 and A_3 are the estimated values of fitting parameters. The data of fitting parameters and SD were tabulated in Table 4.

$$n_D = A_2 + A_3 T \quad (14)$$

Besides that, the RI value can be used to calculate the electronic polarizability or molar refraction (R_m) by applying Lorentz–Lorenz relation as shown in eqn (15) where n_D is representing the RI value and V_m is the molar volume of the APILs. The calculated value of R_m can further be used to obtain free volume (V_f) of APILs, based on eqn (16). V_f is the unoccupied space between molecules which existed due to static and dynamic disorder of the chemical structure.[34] It plays a crucial role for gas solubility in ILs. The V_f can be calculated based on equation.[19,30]

$$R_m = \left(\frac{{n_D}^2 - 1}{{n_D}^2 + 2}\right) V_m \quad (15)$$

$$V_f = V_m - R_m \quad (16)$$

As presented in Table 3, the values of R_m do not show a fixed trend as temperature increases. Thus, it can be concluded that the R_m is not temperature dependent. The same result was obtained by Zhang and co-workers in their study of ether-functionalization ILs coupled with amino acid anion as they concluded this behaviour was due to the induced dipole effect

of ILs.[35] As shown in Table 3, the V_f was found to be directly proportional to APILs's molar mass and increased as temperature increased. Correspondingly, [ETOHA][C5] that has the lowest molar mass owns the lowest V_f value. This is probably due to the small size of $[ETOHA]^+$ cation compared to $[TRIETOHA]^+$ and $[TBA]^+$ thus had contributed into its low V_f.

Viscosity of APILs

In this study, the viscosity of APILs was measured in triplicate at temperature range 293.15–333.15 K. Nonetheless, the viscosity analysis was solely reported by using the water contents as stated in the previous section. The experimental viscosity data is tabulated in the ESI data (Table S3).† Fig. 6 shows the dynamic viscosity of all APILs. Generally, the viscosity of APILs decreased as temperature increased. This is due to the reduction of the binding energy caused by temperature elevation thus increases the mobility of molecules. It was observed that, the viscosity value increased as alkyl chain increased with the exception for ETOHA APILs. According to Chennuri and co-workers, an increased in alkyl chain had resulted in increasing of van der Waals attraction in aliphatic chains which leading into greater dynamic viscosity.[36]

Meanwhile, the opposite trend was observed in viscosity value ETOHA APILs in which [ETOHA][C5] owns higher viscosity value than [ETOHA][C7]. In spite of low molecular force, this may be due to the presence of stronger hydrogen bond in [ETOHA][C5] that overcompensated smaller anion hence contributed to its high viscosity value.[37] Besides that, it had been identified that APILs with $[TBA]^+$ cation own lower viscosity values compared to $[TRIETOHA]^+$ and $[ETOHA]^+$. According to Alcantara *et al.*, the presence of hydroxyl groups in $[TRIETOHA]^+$ and $[ETOHA]^+$ of APILs had increased the polarity of APILs which created a greater ion–ion interaction.[38] This caused the formation of hydrogen bond thus resulting in high viscosity value.

The values of dynamic viscosity were then fitted using eqn (16) as follows:

$$\log \eta = A_4 + A_5/T \quad (17)$$

where η is the value of APILs dynamic viscosity, T is temperature (K) while A_4 and A_5 are the correlation coefficients determined using method of least square. In this study, SD were calculated by using eqn (8).[23] Table 5 shows the estimation of correlated coefficient and SD values calculated by using eqn (8) and (17).

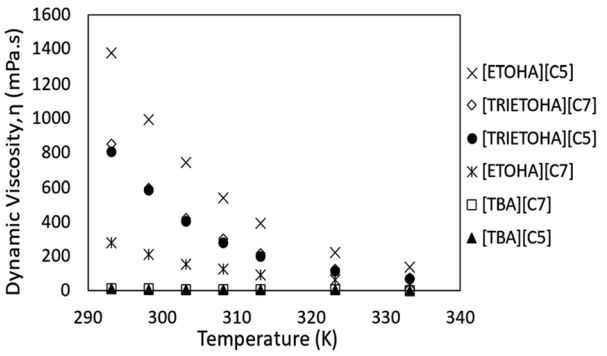

Fig. 6 The dynamic viscosity plot for APILs at temperature range 293.15–308.15 K.

Table 5 Fitting parameters to correlate viscosity of APILs and calculated SD

Ionic liquids	A_4	A_5	SD
[ETOHA][C5]	−5.2774	2463.4	0.0057
[ETOHA][C7]	−4/3744	1993.1	0.0171
[TRIETOHA][C5]	−6.2739	2690.6	0.0130
[TRIETOHA][C7]	−6.0304	2623.6	0.0092
[TBA][C5]	−3.4281	1292.7	0.0195
[TBA][C7]	−3.4998	1332.5	0.0103

Phase transition of APILs

The study on APILs phase transition was carried out by using Differential Scanning Calorimetry (DSC) at the temperature range of −150–80 °C. According to Clough and co-workers, ILs are glass-transforming materials which will not display a freezing point.[39] Except for [TRIETOHA][C7], analysis on DSC thermogram showed the presence of glass transition (T_g) in the temperature range of −77.4 to −114.52 °C for all APILs as shows in Table 6. Meanwhile, the T_g for [TRIETOHA][C7] was not detected within the measured temperature range.

On the other hand, the presence of crystallization (T_c) and melting points (T_m) were detected for APILs with $[TRIETOHA]^+$ cation. Further analysis of the results showed that, T_m increased as anion alkyl chain increased. Besides that, the presence of T_c in [TRIETOHA] APILs could be due to their efficient molecular packing compared to the other APILs. The compactness of $[TRIETOHA]^+$ cation packing is reflected in their density property as both APILs own the largest density value compared [ETOHA] and [TBA] APILs. Meanwhile, the reduction of T_c values was observed as anion alkyl chain increased from [C5] to [C7] which could be due to poor stacking of molecules having relatively longer alkyl chain.

Heat capacity of APILs

The data on the ILs heat capacity (C_p) is vital for estimating the energy consumption during regeneration process, nonetheless very limited data on C_p of ILs is available in literature. Heat capacity is defined as the amount of energy required to increase the temperature of 1 g or 1 mol of substance by 1 K.[40] The C_p of APILs in this study was determined by means of Differential

Table 6 The values of T_g, T_c and T_m for APILs

APILs	T_g (°C)	T_c (°C)	T_m (°C)
[ETOHA][C5]	−79.53	—	—
[ETOHA][C7]	−81.83	—	—
[TRIETOHA][C5]	−70.54	−1.00	8.57
[TRIETOHA][C7]	—	−31.67	11.98
[TBA][C5]	−114.52	—	—
[TBA][C7]	−110.52	—	—

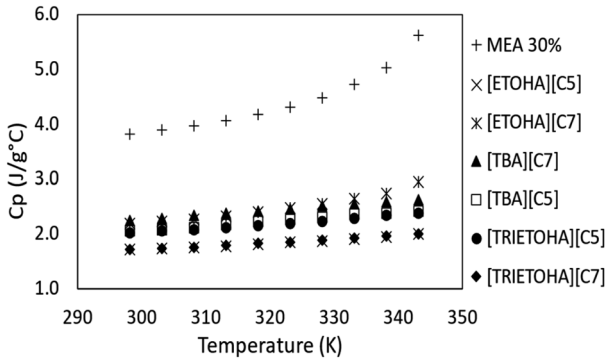

Fig. 7 Heat capacity of APILs and 30% MEA at 298.15–343.15 K.

Scanning Calorimetry (DSC). Fig. 7 shows the C_p for APILs and 30% MEA for comparison purpose. Similar to MEA, the C_p value increases with increasing temperature. Furthermore, the comparison study showed APILs own low C_p compared to MEA. As stated by Xie and co-workers, the overall energy consumption is determined by the C_p value.[41] Ordinarily, solvents with low C_p are much preferable for CO_2 absorption due to low energy consumption compared to MEA.

CO_2 absorption experiment

In this study, the performance of APILs towards CO_2 absorption was analysed in term of mole fraction (X_{CO_2}) and presented in Fig. 8(a) and (b). For clarity, the results are plotted separately according to a common anion. According to Henry's law, the absorption of CO_2 increases with pressure.

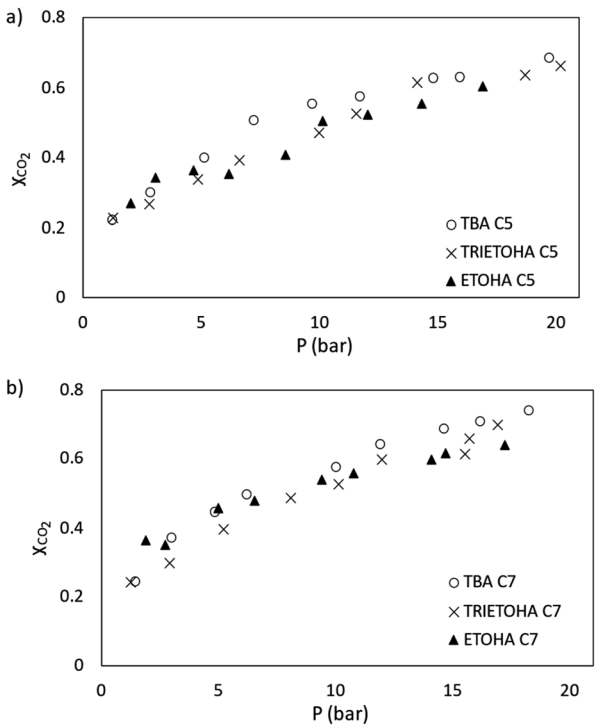

Fig. 8 CO_2 absorption plot for APILs with (a) [C5] and (b) [C7] anions at 298.15 K.

Based on Fig. 8(a) and (b), at 298.15 K with the pressure range from 1–20 bar, the mole fraction of CO_2 (X_{CO_2}) absorbed by APILs was in the range of 0.22 to 0.74. The performance of APILs in CO_2 absorption within the common anion follows the order of [TBA][C7] > [TRIETOHA][C7] > [ETOHA][C7] and [TBA][C5] > [TRIETOHA][C5] > [ETOHA][C5]. For a fixed anion, it was found that APILs with $[TBA]^+$ cation show the highest CO_2 absorption which are 0.69 and 0.74 for [TBA][C5] and [TBA][C7], respectively.

A study by Liu and co-workers confirmed a strong linear correlation between CO_2 solubility in ILs with fractional V_f value.[42] Based on our experimental data, as the molar mass of APILs increased, the V_f value increased as well as the CO_2 absorption capacity of the APILs. In our work, [TBA][C7] with the largest V_f has the highest CO_2 solubility as it provides more space for gas absorption. Additionally, from Fig. 9(a) through (c), a slight increase in CO_2 absorption was observed as anion was shifted from [C5] into [C7]. For example, the mole fraction of CO_2 absorbed by [ETOHA][C5] and [ETOHA][C7] at 20 bar are

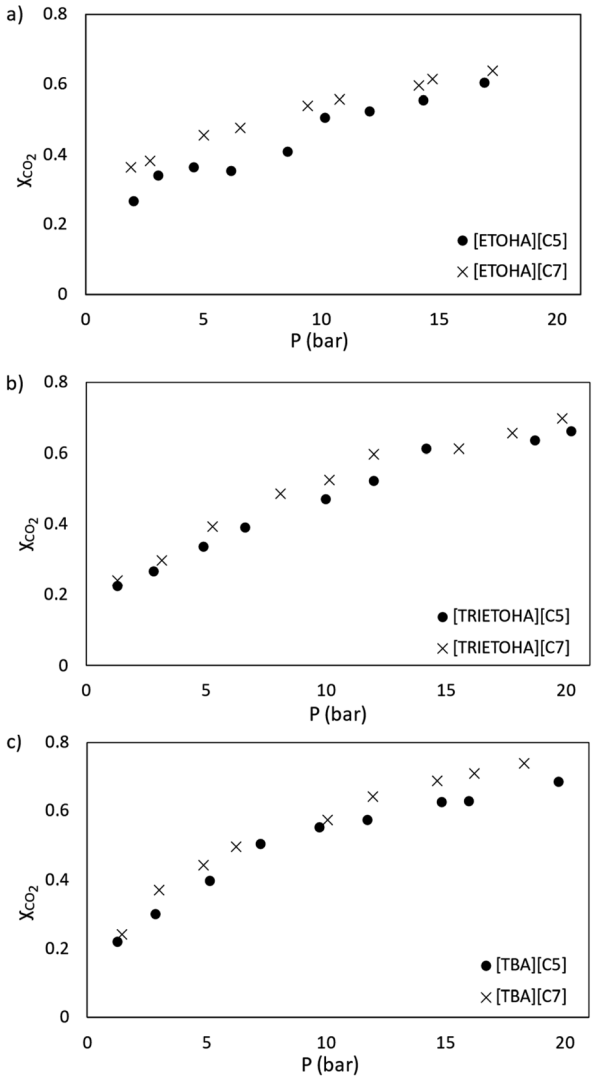

Fig. 9 CO_2 absorption plot for APILs with (a) [ETOHA], (b) [TRIETOHA] and (c) [TBA] cations at 298.15 K.

0.60 and 0.64, correspondingly. The same result was observed on [TRIETOHA] and [TBA]-based APILs. An increase in the anion alkyl chain increased the V_f thus contributed into the overall improvement in the CO_2 solubility of the APIL.

According to Huerstas *et al.*, the absorbing capacity of primary and secondary MEA could reach up to 720 g CO_2 per kg MEA or 72 wt% owing to the hydrolyzation of unstable carbamates to bicarbonate $[HCO_3]^-$.[43] Furthermore, works by Rinprasertmeechai and co-workers have shown that the CO_2 absorption capacity of 30 wt% aqueous MEA was 324 g CO_2 per kg MEA or 32.4 wt% at atmospheric pressure and 298.15 K.[44] Meanwhile, [TBA][C7] recorded 44 g CO_2 per kg IL or 4.4 wt% CO_2 absorption capacity under the same condition which is lower than commercial MEA. Though comparatively the absorption capacity of [TBA][C7] is lower than that of MEA, this somehow shows the potential ability of APILs to be used as solvents for CO_2 removal. However, this result highlight the needs of several improvements before APILs could realistically be utilized in CO_2 removal application.

Table 7 shows the K_H values of APILs calculated based on eqn (6). Generally, the K_H can be obtained through the slope of eqn (6) by assuming that the experimental equilibrium pressure increases linearly with gas solubility in APILs.[45] In this work, the K_H values were calculated in the region of less than 10 bar where the mole fraction of CO_2 is directly proportional to the pressure.

Based on Table 7, it was observed that K_H values increase in the order of [ETOHA][C7] < [ETOHA][C5] < [TBA][C5] < [TBA C7] < [TBA][C7] < [TRIETOHA][C5] < [TRIETOHA][C7]. The values of K_H for APILs in this work are lower than the reported AAILs in which the chemisorption had occurred. This suggests that physical absorption dominates the interactions between CO_2 and APILs in this work.

Comparison of CO_2 absorption with other ILs

There are limited publications on CO_2 solubility in APILs consist of amines cation and carboxylate anion combination. However, for comparison purposes, the present CO_2 solubility data was compared with several developed ILs namely 1-hexyl-3-methylimidazolium bis(trifluoromethylsulfonyl)imide [HMIM][NTf_2], 1-butyl-4-methyl pyridinium arginate [B_4MPyr][L-Arg],[46] choline arginate [Cho][Arg][47] and *N*,*N*-diethanolammonium pentanoate [DEEA][Pent].[45] It has been observed that, the CO_2 absorption by APILs displayed a remarkable performance in comparison to traditional [HMIM][NTf_2]. For example, [TBA][C7] recorded 0.736 mole fraction of CO_2 at 20 bar, 298.15 K while [HMIM][NTf_2] demonstrated 0.415 absorption capacity at the same conditions. Research by Noorani *et al.* demonstrated that their amino acid based-IL, 1-butyl-4-methyl pyridinium arginate [BMPyr][L-Arg] recorded the value of 0.594 CO_2 mole fraction at 6 bar, 298.15 K.[46] The same authors also synthesized choline based ILs coupled with amino acid anion. It was observed that the CO_2 absorption capacity by choline arginate [Cho][Arg] was 0.552 mole fraction at 3 bar, 298.15 K. Higher CO_2 solubility in AAILs compared to APILs could be contributed to the presence of two amines group in AAILs structure thus allowing more sites for gas absorption. Nonetheless, the best comparison can be made by comparing [TRIETOHA][C5] and [TBA][C5] with [DEEA][Pent] as they have common combination of tertiary amine and carboxylic acid. Based on Fig. 10, the CO_2 absorption data for [TRIETOHA][C5], [TBA][C5] and [DEAA][Pent] show the same trend in which the mole fraction of CO_2 absorbed is directly proportional to gas pressure.

Table 7 The K_H values of APILs at 298.15 K

APILs	K_H (bar)
[ETOHA][C5]	16.19
[ETOHA][C7]	14.12
[TRIETOHA][C5]	40.53
[TRIETOHA][C7]	30.08
[TBA][C5]	18.86
[TBA][C7]	27.59
[B_4MPyr][L-Arg]	121.88 (ref. 46)

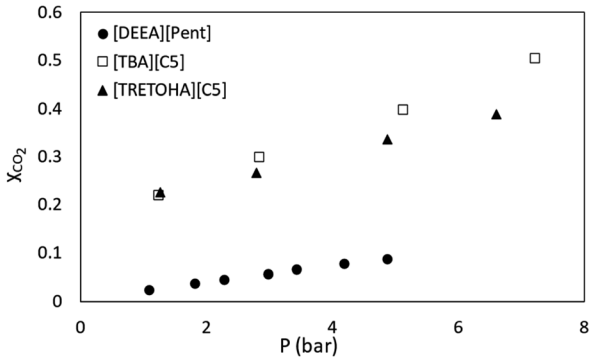

Fig. 10 Comparison of CO_2 absorption in APILs, [TBA][C5] and [TRIETOHA][C5] at 298.15 K with [DEEA][Pent] at 303 K by Silva *et al.*[45]

Characterization of APILs after CO_2 absorption

In this work, FTIR and ^{13}C NMR spectroscopy were used to study the possible CO_2 absorption pathway by APILs. Analysis conducted on ^{13}C NMR of [TBA][C7] as shown in Fig. 11 shows the absence of any new peak in [TBA][C7]-CO_2. Besides that, FTIR analysis was done by employing attenuated total reflectance (ATR) sampling technique in the region of 4000–450 cm^{-1} under 16 scans. Fig. 12 shows the comparison of the FTIR spectra for [TBA][C7] before and after CO_2 absorption while the FTIR spectra for [ETOHA][C5], [ETOHA][C7], [TRIETOHA][C5], [TRIETOHA][C7] and [TBA][C5] are presented in the ESI data.† In general, the aliphatic amine (–NH) was observed at 2922–2954 cm^{-1}. The C–H of alkane is depicted at 2856–2871 cm^{-1}. The COO– of carboxylate anion can be assigned at 1526–1586 cm^{-1}. Furthermore, peaks at 1071–1068 cm^{-1} represent primary alcohol, OH of $[ETOHA]^+$ and $[TRIETOHA]^+$ cations. Meanwhile, the FTIR spectra of APILs after gas absorption show the presence of a new peak at around 2334–2336 cm^{-1}, associated with O=C=O thus indicates the existence of CO_2 in APILs. Besides that, there are no formation of new peaks in the area corresponds to carbonyl of carbamate which is usually shown in the case of chemisorption mechanism. Therefore, these results

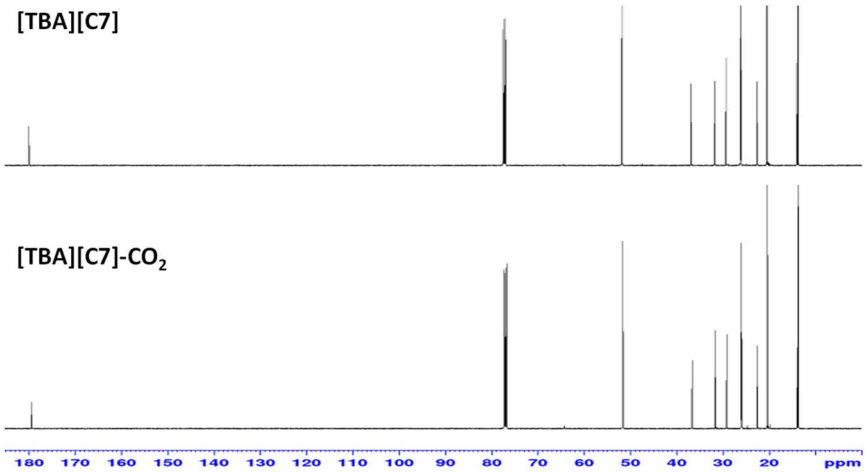

Fig. 11 ^{13}C NMR for [TBA][C7] before and after CO_2 absorption.

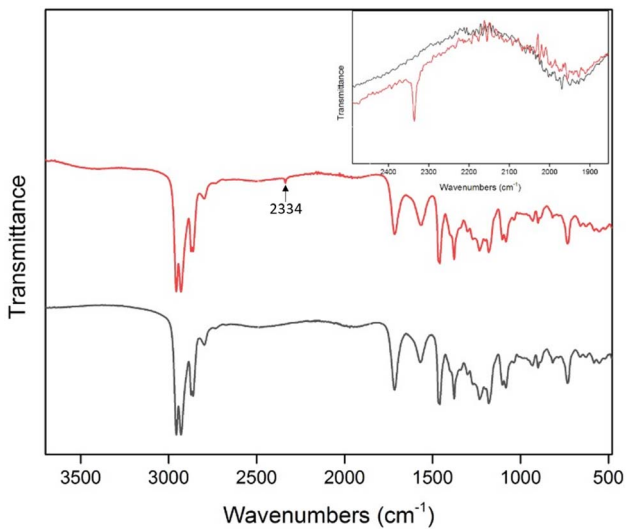

Fig. 12 FTIR spectra for [TBA][C7], before and after CO_2 absorption. (—) Black and (—) red denote before and after absorption, respectively. Inset figure shows the wavenumbers in the region approximately 2300 cm^{-1} to highlight the presence of CO_2 in [TBA][C7].

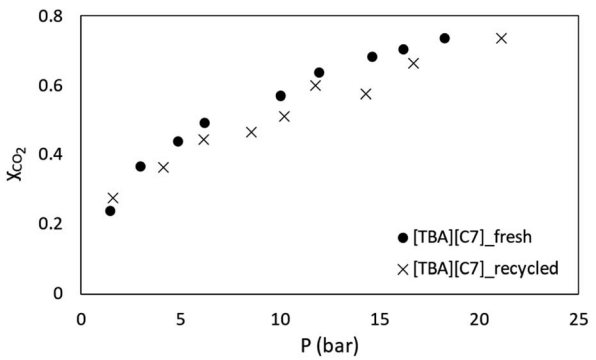

Fig. 13 CO_2 absorption plot for fresh and recycled [TBA][C7] at 298.15 K.

manifest that the CO_2 absorption in APILs is solely based on physisorption interaction.

Recyclability of APILs for CO_2 absorption

Besides that, the study on recyclability of APILs towards CO_2 absorption was also conducted. In this work, APIL [TBA][C7] that has recorded the highest CO_2 solubility was selected to be used in the recyclability study. This preliminary recyclability study was conducted in a single cycle only. Used [TBA][C7] was placed under vacuum for 2 hours at 60 °C to remove absorbed CO_2 before being utilized in a new cycle of absorption. In the meantime, Fig. 13 shows the data of CO_2 absorption in fresh and recycled [TBA][C7]. The plot indicates a marginal difference in the absorption capacity of CO_2 between fresh and recycled [TBA][C7] thus suggesting that the APIL indicates a good potential to be used several times in absorbing CO_2.

However, one should take note on the high energy and cost incurred with the utilization of vacuum during recyclability process. Therefore, it is crucial to further explore other methods with comparatively lower energy usage than that of vacuum such as pressure, thermal and electric swing techniques for recyclability study of the ILs.

Conclusions

In this work, six APILs were successfully synthesized, characterized and utilized for CO_2 absorption study. The study indicates that APILs have lower C_p value compared to commonly used MEA thus providing low energy consumption during recyclability process. Further analysis on APILs physiochemical properties also revealed that, their molar masses provide significant effect towards V_m, V, $S°$, U_{POT} and V_f values. Other than that, it has been observed that V_f is the key factor in determining the capability of APILs in CO_2 absorption in which [TBA][C7] with the largest V_f recorded the highest mole fraction of absorbed CO_2. The experimental values of CO_2 absorption were utilized in K_H determination which in turn have revealed that the CO_2 absorption in APILs is attributed by physisorption

interaction. This deduction was supported by ^{13}C NMR and FTIR analyses in view of the absence of new peaks related to the formation of carbamate species. The recyclability study conducted at one cycle shows an insignificant reduction in CO_2 solubility in [TBA][C7] thus suggesting the promising performance of APILs as liquid absorbents. Nevertheless, in this preliminary study of APIL recyclability, high energy vacuum system was used. Hence, it is of utmost important in the future to focus on the development of new alternatives utilize low energy yet effective in ILs recyclability for CO_2 capture.

Author contribution

A. H. A. R.: investigation, formal analysis, data curation, methodology and writing-original draft. N. M. Y., N. A. G. and M. U.: conceptualization, N. M. Y.: supervision, funding acquisition, validation, and writing-review and editing. Z. J. M. F. A., N. H. Z. O. Z., S. A. M. F.: methodology and investigation.

Conflicts of interest

There are no conflicts to declare.

Acknowledgements

The authors would like to acknowledge the financial fund provided by International Collaborative Research Funding (ICRF) between Universiti Teknologi PETRONAS and Universitas Islam Riau (UTP-UIR) with the cost center number of 015ME0-165 for this project. Financial assistance and support from Universiti Teknologi PETRONAS and Centre for Research in Ionic Liquid (CORIL), UTP, are greatly acknowledged.

References

1 A. Safari, N. Das, O. Langhelle, J. Roy and M. Assadi, *Energy Sci. Eng.*, 2019, **7**, 1075–1094.
2 A. B. Wasiu, A. R. A. Aziz and M. R. Heikal, *J. Appl. Sci.*, 2012, **12**, 2345–2350.
3 N. Ghasem, in *Advances in Carbon Capture*, Elsevier, 2020, pp. 479–501.
4 F. Vega, M. Cano, S. Camino, L. M. G. Fernández, E. Portillo and B. Navarrete, *Carbon Dioxide Chemistry, Capture and Oil Recovery*, 2018, pp. 142–163.
5 M. Hasib-ur-Rahman, M. Siaj and F. Larachi, *Chem. Eng. Process. Process Intensif.*, 2010, **49**, 313–322.
6 R. Dawson, L. A. Stevens, O. S. Williams, W. Wang, B. O. Carter, S. Sutton, T. C. Drage, F. Blanc, D. J. Adams and A. I. Cooper, *Energy Environ. Sci.*, 2014, **7**, 1786–1791.
7 P. Nancarrow and H. Mohammed, *ChemBioEng Rev.*, 2017, **4**, 106–119.
8 F. U. Shah, R. An and N. Muhammad, *Front. Chem.*, 2020, **8**, 1–3.
9 A. Tagiuri, K. Z. Sumon and A. Henni, *Fluid Phase Equilib.*, 2014, **380**, 39–47.
10 N. M. Yunus, M. A. Mutalib, Z. Man, M. A. Bustam and T. Murugesan, *Chem. Eng. J.*, 2012, **189**, 94–100.
11 B.-C. Lee and S. G. Nam, *Korean J. Chem. Eng.*, 2015, **32**, 521–533.
12 S. Babamohammadi, A. Shamiri and M. K. Aroua, *Rev. Chem. Eng.*, 2015, **31**, 383–412.
13 M. Ghorbani and M. I. Simone, *ACS Omega*, 2020, **5**, 12637–12648.
14 K. Fukumoto, M. Yoshizawa and H. Ohno, *J. Am. Chem. Soc.*, 2005, **127**, 2398–2399.
15 S. Kang, Y. G. Chung, J. H. Kang and H. Song, *J. Mol. Liq.*, 2020, **297**, 111825.
16 S. Saravanamurugan, A. J. Kunov-Kruse, R. Fehrmann and A. Riisager, *ChemSusChem*, 2014, **7**, 897–902.
17 M. Rezaeian, M. Izadyar and A. Nakhaei Pour, *J. Phys. Chem. A*, 2018, **122**, 5721–5729.
18 M. Przypis, K. Matuszek, A. Chrobok, M. Swadźba-Kwaśny and D. Gillner, *J. Mol. Liq.*, 2020, **308**, 113166.
19 T. L. Greaves and C. J. Drummond, *Chem. Rev.*, 2008, **108**, 206–237.
20 N. M. Yunus, N. H. Halim, C. D. Wilfred, T. Murugesan, J. W. Lim and P. L. Show, *Processes*, 2019, **7**, 820.
21 F. Li, Y. Bai, S. Zeng, X. Liang, H. Wang, F. Huo and X. Zhang, *Int. J. Greenhouse Gas Control*, 2019, **90**, 102801.
22 P. K. Chhotaray, S. Jella and R. L. Gardas, *J. Chem. Thermodyn*, 2014, **74**, 255–262.
23 N. H. Z. Othman Zailani, N. M. Yunus, A. H. Ab Rahim and M. A. Bustam, *Processes*, 2020, **8**, 742.
24 Y. Cao and T. Mu, *Ind. Eng. Chem. Res.*, 2014, **53**, 8651–8664.
25 D. Santos, M. Santos, E. Franceschi, C. u. Dariva, A. Barison and S. Mattedi, *J. Chem. Eng. Data*, 2016, **61**, 348–353.
26 R. Gusain, S. Panda, P. S. Bakshi, R. L. Gardas and O. P. Khatri, *J. Mol. Liq.*, 2018, **269**, 540–546.
27 M. Montalbán, C. Bolívar, F. G. Diaz Banos and G. Víllora, *J. Chem. Eng. Data*, 2015, **60**, 1986–1996.
28 F. Yang and P. Feng, *Appl. Sci.*, 2020, **10**, 8342.
29 D. Keshapolla, K. Srinivasarao and R. L. Gardas, *J. Chem. Thermodyn*, 2019, **133**, 170–180.
30 A. S. Khan, Z. Man, A. Arvina, M. A. Bustam, A. Nasrullah, Z. Ullah, A. Sarwono and N. Muhammad, *J. Mol. Liq.*, 2017, **227**, 98–105.
31 R. L. Gardas, H. F. Costa, M. G. Freire, P. J. Carvalho, I. M. Marrucho, I. M. Fonseca, A. G. Ferreira and J. A. Coutinho, *J. Chem. Eng. Data*, 2008, **53**, 805–811.
32 Ł. Marcinkowski, E. Szepiński, M. J. Milewska and A. Kloskowski, *J. Mol. Liq.*, 2019, **284**, 557–568.
33 S. Seki, S. Tsuzuki, K. Hayamizu, Y. Umebayashi, N. Serizawa, K. Takei and H. Miyashiro, *J. Chem. Eng. Data*, 2012, **57**, 2211–2216.
34 Y. Yu and Y. Chen, *ACS Omega*, 2021, **6**, 14869–14874.
35 D. Zhang, B. Li, M. Hong, Y.-X. Kong, J. Tong and W.-G. Xu, *J. Mol. Liq.*, 2020, **304**, 112718.
36 B. K. Chennuri, V. Losetty, C. D. Wilfred and R. L. Gardas, *J. Mol. Liq.*, 2017, **241**, 246–254.
37 P. Bonhote, A.-P. Dias, N. Papageorgiou, K. Kalyanasundaram and M. Grätzel, *Inorg. Chem.*, 1996, **35**, 1168–1178.
38 M. L. Alcantara, J. P. Santos, M. Loreno, P. I. Ferreira, M. L. Paredes, L. Cardozo-Filho, A. K. Silva, L. M. Liao,

C. A. Pires and S. Mattedi, *Fluid Phase Equilib.*, 2018, **459**, 30–43.
39 M. T. Clough, C. R. Crick, J. Gräsvik, P. A. Hunt, H. Niedermeyer, T. Welton and O. P. Whitaker, *Chem. Sci.*, 2015, **6**, 1101–1114.
40 E. Gómez, N. Calvar and Á. Domínguez, *Ionic Liquids-Current State of the Art*, 2015, vol. 20, pp. 199–228.
41 Y. Xie, Y. Zhang, X. Lu and X. Ji, *Appl. Energy*, 2014, **136**, 325–335.
42 X. Liu, K. E. O'Harra, J. E. Bara and C. H. Turner, *Phys. Chem. Chem. Phys.*, 2020, **22**, 20618–20633.
43 J. I. Huertas, M. D. Gomez, N. Giraldo and J. Garzón, *J. Chem.*, 2015, **2015**, 1–7.
44 S. Rinprasertmeechai, S. Chavadej, P. Rangsunvigit and S. Kulprathipanja, *Int. J. Chem. mol. Eng.*, 2012, **6**, 284–288.
45 L. P. Silva, E. A. Crespo, M. A. Martins, P. C. Barbosa, R. L. Gardas, L. F. Vega, J. o. A. Coutinho and P. J. Carvalho, *Ind. Eng. Chem. Res.*, 2022, **61**, 4046–4057.
46 N. Noorani, A. Mehrdad and I. Ahadzadeh, *Fluid Phase Equilib.*, 2021, **547**, 113185.
47 N. Noorani and A. Mehrdad, *J. Mol. Liq.*, 2022, **357**, 119078.